

# From scattering or impedance matrices to Bloch modes of photonic crystals

Boris Gralak, Stefan Enoch, and Gérard Tayeb

*Institut Fresnel, Case 262, Faculté des Sciences et Techniques, Centre de St Jérôme,  
13397 Marseille Cedex 20, France*

Received September 24, 2001; revised manuscript received January 7, 2002; accepted February 7, 2002

The dispersion relation of Bloch waves is derived from the properties of a single grating layer. A straightforward way to impose the Bloch condition leads to the calculation of the eigenvalues of the transfer matrix through the single grating layer. Unfortunately, the transfer-matrix algorithm is known to be unstable as a result of the growing evanescent waves. This problem appears again in the calculation of the eigenvalues, making unusable the transfer matrix in numerous practical problems. We propose two different algorithms to circumvent this problem. The first one takes advantage of scattering matrices, while the second one takes advantage of impedance matrices. Numerical evidence of the efficiency of the algorithms is given. Dispersion diagrams of simple cubic and woodpile photonic crystals are obtained by using, respectively, the scattering and impedance matrices. © 2002 Optical Society of America

OCIS codes: 050.1950, 260.2110.

## 1. INTRODUCTION

Photonic crystals are dielectric or metallic structures whose dielectric permittivity varies periodically in space.

The most interesting property of photonic crystals is their ability to shape the dispersion relation, and the most famous consequence is the existence of bandgaps for proper parameters of the crystal (permittivity, filling ratio). The full bandgaps, i.e., the frequency intervals where no electromagnetic wave can propagate in the photonic crystal whatever the polarization and the direction of propagation, was the first motivation of earlier work. The aim was to inhibit spontaneous emission responsible, for example, for the laser threshold in laser diodes.

Increasingly, it appears that one key feature is the numerical computation of the dispersion relation of the Bloch modes, which gives synthetic information on the propagation of the light in the crystal. Thus the calculation of the dispersion relation of Bloch modes has been the subject of intensive research, and several methods have emerged from this scientific agitation, such as the plane-wave method,<sup>1,2</sup> the transfer-matrix method,<sup>3</sup> the Korringa-Kohn-Rostoker method,<sup>4,5</sup> and the multipole method.<sup>6</sup>

Another approach is to interpret a photonic crystal as a stack of identical periodic layers. This way has been investigated recently, for photonic crystals, by several groups, including the authors of the present paper,<sup>7</sup> Botten *et al.*,<sup>8</sup> Modinos *et al.*,<sup>9</sup> and Whittaker.<sup>10</sup> As the periodic layers are nothing but gratings, we can profit from the large amount of work in the electromagnetic theory of gratings. Indeed, grating structures have been studied theoretically since early in the 1960s.<sup>11</sup> If the first application is spectroscopy, it emerges that numerous devices in modern optics require gratings: Grating couplers were deeply studied for distributed-feedback lasers<sup>12</sup> or second-harmonic-generation enhancement.<sup>13</sup> Many efficient methods have been developed, such as integral,<sup>14</sup>

differential,<sup>15,16</sup> and modal methods,<sup>17–20</sup> and are now mature. There are strong points in favor of this approach: It can deal with dispersive and absorptive materials without any difficulties, requires no huge computational resources if the grating method used is a good one, and is rapidly convergent and accurate.

In our previous paper,<sup>7</sup> we give a simple interpretation in terms of a grating transfer matrix, and we obtain the dispersion relation from this matrix in combination with the Bloch theorem. Unfortunately, this approach suffers from numerical instabilities in some practical problems. Botten *et al.* have proposed a formulation for two-dimensional (2D) rectangular, centered rectangular, or hexagonal crystals that, taking advantage of the up-down symmetry of the crystal,<sup>8</sup> does not suffer from numerical instability. However, to our knowledge, no algorithm has been proposed in the general, three-dimensional (3D) case (where the up-down symmetry does not exist) to deduce the dispersion relation from the properties of a grating layer without any numerical instabilities.

First, from the Bloch theorem and the transfer-matrix definition, an expression for the dispersion relation is given. Then the origin of the numerical instabilities is sketched, and we propose our solutions. We propose two algorithms to compute the dispersion relation. In the first, we develop an eigenvalue problem from the impedance, or  $R$ , matrix, while in the second the eigenvalue problem uses the scattering, or  $S$ , matrix.<sup>21</sup>

The numerical efficiency of the algorithms is illustrated with the actual structures of simple cubic and face-centered-cubic woodpile photonic crystals fabricated by Lin *et al.*<sup>22,23</sup> It is shown that the  $R$ -matrix algorithm associated with a rigorous modal method<sup>17–20</sup> allows us to obtain a very accurate dispersion relation for the woodpile structure with a computational burden close to that of 2D structures. The simple cubic structure is studied by us-

ing the coupled waves or the Fourier modal method<sup>24</sup> combined with the  $S$ -matrix algorithm. Then it is shown that the computed dispersion relation fits the experimental results of Ref. 25 and the transmission curves. Thus the discrepancy between the transmission curves and the dispersion relation observed in Ref. 25 can be attributed to the slow convergence of the plane-wave method<sup>26</sup> rather than to a limited size effect.

## 2. BLOCH BOUNDARY CONDITION AND GRATING LAYERS

We begin by defining appropriate notation.

### A. Geometry

Let us consider a 3D photonic crystal with spatial periods  $\mathbf{d}_1$ ,  $\mathbf{d}_2$ , and  $\mathbf{d}_3$  [Fig. 1(a)]. Note that this basis is not supposed to be orthogonal. In the following, we use the coordinate system associated with the basis  $(\mathbf{d}_1, \mathbf{d}_2, \mathbf{d}_3)$ . The unit cell  $V$  and the lattice  $L$  of this crystal are

$$\begin{aligned} V &= \{\mathbf{x} = x_1\mathbf{d}_1 + x_2\mathbf{d}_2 + x_3\mathbf{d}_3 \in \mathbb{R}^3 | x_1, x_2, x_3 \in [0,1]\}, \\ L &= \{\boldsymbol{\gamma} = \gamma_1\mathbf{d}_1 + \gamma_2\mathbf{d}_2 + \gamma_3\mathbf{d}_3 \in \mathbb{R}^3 | \gamma_1, \gamma_2, \gamma_3 \in \mathbb{Z}\}. \end{aligned} \quad (1)$$

The volume of this unit cell is denoted by  $|V|$ . The vectors of the basis of the dual lattice are

$$\begin{aligned} \mathbf{d}_1^* &= (2\pi/|V|)\mathbf{d}_2 \times \mathbf{d}_3, \\ \mathbf{d}_2^* &= (2\pi/|V|)\mathbf{d}_3 \times \mathbf{d}_1, \\ \mathbf{d}_3^* &= (2\pi/|V|)\mathbf{d}_1 \times \mathbf{d}_2. \end{aligned} \quad (2)$$

The permeability is assumed to be equal to that of vacuum,  $\mu_0$ , and the permittivity  $\epsilon$  has the periodicity of the lattice  $L$ :

$$\forall \mathbf{x} \in \mathbb{R}^3, \forall \boldsymbol{\gamma} \in L: \epsilon(\mathbf{x} + \boldsymbol{\gamma}) = \epsilon(\mathbf{x}). \quad (3)$$

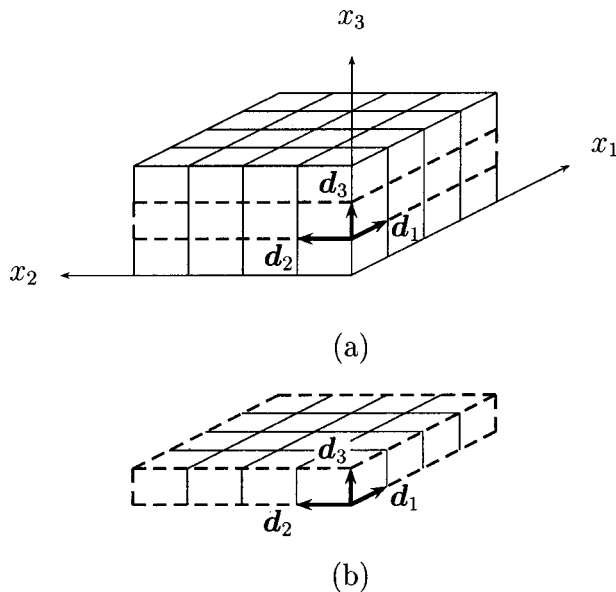


Fig. 1. (a) 3D photonic crystal with spatial periods  $\mathbf{d}_1$ ,  $\mathbf{d}_2$ , and  $\mathbf{d}_3$ , (b) grating layer extracted from this 3D crystal with spatial periods  $\mathbf{d}_1$  and  $\mathbf{d}_2$ .

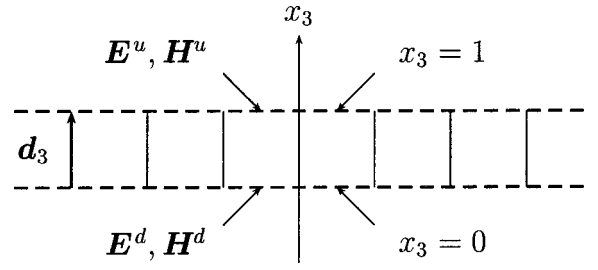


Fig. 2. Value of the electromagnetic field at the planes  $x_3 = 0$  and  $x_3 = 1$  delimiting the grating layer.

This photonic crystal can be seen as an infinite stack of identical grating layers. Each of these grating layers is 2D periodic with spatial periods  $\mathbf{d}_1$  and  $\mathbf{d}_2$  and is deduced from the adjacent one by a translation of  $\pm\mathbf{d}_3$  [Fig. 1(b)].

### B. Electromagnetic Field

First, we consider the isolated grating layer located between the planes  $x_3 = 0$  and  $x_3 = 1$  (Fig. 2). The electromagnetic field is assumed to have the time-harmonic dependence  $\exp(-i\omega t)$ . Because of the 2D periodicity of the grating layer, we can perform the usual partial Bloch reduction. In this case, the electromagnetic field, represented by its complex amplitude  $(\mathbf{E}, \mathbf{H})$ , satisfies the partial, or 2D, Bloch boundary condition, known as the pseudoperiodicity condition in grating theory. For all  $\mathbf{x} \in \mathbb{R}^3$  and for all  $n_1$  and  $n_2 \in \mathbb{Z}$ , we have

$$\mathbf{F}(\mathbf{x} + n_1\mathbf{d}_1 + n_2\mathbf{d}_2) = \exp[i\mathbf{k} \cdot (n_1\mathbf{d}_1 + n_2\mathbf{d}_2)]\mathbf{F}(\mathbf{x}), \quad (4)$$

where  $\mathbf{F} = \mathbf{E}, \mathbf{H}$  and

$$\begin{aligned} \mathbf{k} \in V^* &= \{k_1\mathbf{d}_1^* + k_2\mathbf{d}_2^* + k_3\mathbf{d}_3^* \in \mathbb{R}^3 | k_1, k_2, k_3 \\ &\in [-1/2, 1/2]\} \end{aligned} \quad (5)$$

is the Bloch wave vector in the unit cell of the dual lattice.

We denote by  $(\mathbf{E}^u, \mathbf{H}^u)$  and  $(\mathbf{E}^d, \mathbf{H}^d)$  the field at the planes delimiting the grating layer (Fig. 2):

$$\begin{aligned} \mathbf{F}^u(x_1, x_2) &= \mathbf{F}(x_1, x_2, 1), \\ \mathbf{F}^d(x_1, x_2) &= \mathbf{F}(x_1, x_2, 0), \end{aligned} \quad (6)$$

where  $\mathbf{F} = \mathbf{E}, \mathbf{H}$ . The partial Bloch boundary condition, or pseudoperiodicity, allows us to develop the functions  $\mathbf{E}^u, \mathbf{H}^u, \mathbf{E}^d$ , and  $\mathbf{H}^d$  by using the Fourier basis:

$$\begin{aligned} \mathbf{F}^\sigma(x_1, x_2) &= \sum_{n_1, n_2 \in \mathbb{Z}} \mathbf{F}_{n_1, n_2}^\sigma \exp[i(k_1 + n_1)x_1] \\ &\quad \times \exp[i(k_2 + n_2)x_2], \end{aligned} \quad (7)$$

where, for all  $\mathbf{F} = \mathbf{E}, \mathbf{H}$  and  $\sigma = u, d$ ,

$$\mathbf{F}_{n_1, n_2}^\sigma = F_{1, n_1, n_2}^\sigma \mathbf{d}_1 + F_{2, n_1, n_2}^\sigma \mathbf{d}_2 + F_{3, n_1, n_2}^\sigma \mathbf{d}_3 \in \mathbb{C}^3. \quad (8)$$

We denote by  $F^\sigma$  the infinite column vector defining the tangential components  $F_1^\sigma$  and  $F_2^\sigma$  of the vectorial functions  $\mathbf{F}^\sigma$  for all  $F = E, H$  and  $\sigma = u, d$ :

$$F^\sigma = \begin{pmatrix} F_{1, n_1, n_2}^\sigma \\ F_{2, n_1, n_2}^\sigma \end{pmatrix}_{n_1, n_2 \in \mathbb{Z}} \quad (9)$$

Finally, as is well-known in grating theory, the numerical resolution of Maxwell's equations gives us a transfer-matrix relationship between the tangential components of the field on the upper and lower interfaces:

$$\begin{pmatrix} E^u \\ H^u \end{pmatrix} = T(\omega, k_1, k_2) \begin{pmatrix} E^d \\ H^d \end{pmatrix}, \quad (10)$$

where  $T(\omega, k_1, k_2)$  is the transfer matrix for given values of  $\omega$ ,  $k_1$ , and  $k_2$ .

### C. Dispersion Relation

Now let us return to the 3D photonic crystal and link the grating layer transfer matrix to the dispersion relation of the 3D crystal. A Bloch mode in this 3D photonic crystal satisfies the total, or 3D, Bloch condition. To fulfill the total Bloch condition, we have to add a supplementary condition to the previous one [Eq. (4)]. From Eqs. (6), (7), and (9), we obtain the following for all  $\mathbf{x} \in \mathbb{R}^3$  and for all  $n_3 \in \mathbb{Z}$ :

$$\begin{pmatrix} E^u \\ H^u \end{pmatrix} = \exp(i\mathbf{k} \cdot \mathbf{d}_3) \begin{pmatrix} E^d \\ H^d \end{pmatrix}. \quad (11)$$

From Eqs. (10) and (11), it appears that the total Bloch condition is satisfied if the scalar  $\exp(i\mathbf{k} \cdot \mathbf{d}_3)$  is an eigenvalue of the transfer matrix. The expression for the dispersion relation is then

$$\det[T(\omega, k_1, k_2) - I \exp(i\mathbf{k} \cdot \mathbf{d}_3)] = 0, \quad (12)$$

where  $I$  is the identity matrix.

Unfortunately, the numerical computation of the eigenvalues of the transfer matrix is unstable because of the growing evanescent waves. These eigenvalues tend exponentially to infinity or zero when the size of the truncated transfer matrix increases. So expression (12) for the dispersion relation is, in numerous practical problems, unusable.

In Section 3, we propose stable algorithms to compute these eigenvalues from scattering (or  $S$ ) and impedance (or  $R$ ) matrices.

## 3. STABLE ALGORITHMS

One of the more significant recent advances in the electromagnetic theory of gratings was the formulation of stable propagation algorithms.<sup>21,27,28</sup> We can divide all these algorithms into two categories:  $S$ - and  $R$ -matrix algorithms.

First, we present the main idea of our stable algorithm. Numerical instabilities are due to the behavior of the eigenvalues  $\{\lambda_n | n \in \mathbb{N}\}$  of the  $T$  matrix. When the size of the truncated  $T$  matrix increases, some of the eigenvalues tend exponentially to infinity while others tend exponentially to zero. Inverting the  $T$  matrix can solve the problem due to the growing eigenvalues, but the ones close to zero cause the same growing behavior for the eigenvalues of the matrix  $T^{-1}$ .

Hence we first add the identity matrix  $\pm I$  to the  $T$  matrix. This matrix  $(T \pm I)$  has the same eigenvectors as those of  $T$ , and its eigenvalues are  $\{\lambda_n \pm 1 | n \in \mathbb{N}\}$ . So no eigenvalues of this new matrix  $(T \pm I)$  tend to zero. Second, we consider the matrix  $(T \pm I)^{-1}$ . Again, this new matrix  $[(T \pm I)^{-1}]$  has the same eigenvectors as

those above, and its eigenvalues are  $\{(\lambda_n \pm 1)^{-1} | n \in \mathbb{N}\}$ . Now none of these eigenvalues tends to infinity. So no numerical instabilities are expected. The dispersion relation (12) is equivalent to

$$\det\{[T(\omega, k_1, k_2) \pm I]^{-1} - I[\exp(i\mathbf{k} \cdot \mathbf{d}_3) \pm 1]^{-1}\} = 0. \quad (13)$$

Note that the two possibilities linked to the  $\pm$  sign will give the same result, except when there are eigenvalues equal to  $\pm 1$ . In this particular case, one of the two dispersion relations is well conditioned and allows us to get the correct eigenvalues. In the very improbable case where both  $+1$  and  $-1$  are eigenvalues of  $T$ , one can add to  $T$  any matrix  $aI$ , where  $a$  is an arbitrary complex number. In our numerical experience, we have never encountered such circumstances.

The next step is to derive an expression for the matrix  $(T \pm I)^{-1}$  from the matrix  $R$  or  $S$ , paying attention to numerical instabilities.

### A. Stable Algorithm from Impedance (or $R$ ) Matrix

We denote by  $R$  the impedance matrix. This matrix links the vectors  $E^u$  and  $E^d$  [Eq. (9)] to the vectors  $H^u$  and  $H^d$  (Ref. 21):

$$\begin{pmatrix} E^u \\ E^d \end{pmatrix} = R(\omega, k_1, k_2) \begin{pmatrix} H^u \\ H^d \end{pmatrix} = \begin{bmatrix} R_{11} & R_{12} \\ R_{21} & R_{22} \end{bmatrix} \begin{pmatrix} H^u \\ H^d \end{pmatrix}, \quad (14)$$

where  $R_{11}$ ,  $R_{12}$ ,  $R_{21}$ , and  $R_{22}$  are the four submatrices of the matrix  $R$ . After tedious but straightforward calculation, we derive from Eqs. (10) and (14) the expression for the matrix  $(T \pm I)^{-1}$ :

$$\begin{aligned} (T \pm I)^{-1} &= \begin{bmatrix} (R_{22} \mp R_{21})X & (R_{22} \mp R_{21})XY(R_{22} \mp R_{21})^{-1}R_{22} \\ X & -X(R_{11} \pm R_{21}) \end{bmatrix}, \end{aligned} \quad (15)$$

where

$$\begin{aligned} X &= [(R_{12} - R_{21}) \pm (R_{22} - R_{11})]^{-1}, \\ Y &= R_{12}R_{22}^{-1}R_{21} - R_{11}. \end{aligned} \quad (16)$$

### B. Stable Algorithm from Scattering (or $S$ ) Matrix

The  $S$  matrix gives a relationship between incoming and outgoing waves around the grating layer<sup>21</sup> (Fig. 3). To define this  $S$  matrix, we have to develop the electric field above and below the grating layer on the plane-wave basis, which is convenient for separating incoming and out-

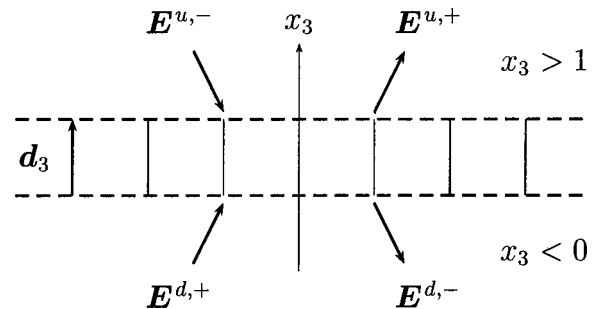


Fig. 3. Definition of the  $S$  matrix.

going waves. For this purpose, we assume that the vectorial function  $\mathbf{E}$  can be written as a Rayleigh series<sup>29</sup>:

For  $x_3 > 1$ ,

$$\mathbf{E}(\mathbf{x}) = \sum_{n_1, n_2 \in \mathbb{Z}} [\mathbf{E}_{n_1, n_2}^{u, +} \exp(i\mathbf{k}_{n_1, n_2}^+ \cdot \mathbf{x}) + \mathbf{E}_{n_1, n_2}^{u, -} \exp(i\mathbf{k}_{n_1, n_2}^- \cdot \mathbf{x})]$$

For  $x_3 < 0$ ,

$$\mathbf{E}(\mathbf{x}) = \sum_{n_1, n_2 \in \mathbb{Z}} [\mathbf{E}_{n_1, n_2}^{d, +} \exp(i\mathbf{k}_{n_1, n_2}^+ \cdot \mathbf{x}) + \mathbf{E}_{n_1, n_2}^{d, -} \exp(i\mathbf{k}_{n_1, n_2}^- \cdot \mathbf{x})] \quad (17)$$

where, for all  $\sigma = u, d$ ,

$$\mathbf{E}_{n_1, n_2}^{\sigma, \pm} = E_{1, n_1, n_2}^{\sigma, \pm} \mathbf{d}_1 + E_{2, n_1, n_2}^{\sigma, \pm} \mathbf{d}_2 + E_{3, n_1, n_2}^{\sigma, \pm} \mathbf{d}_3 \in \mathbb{C}^3,$$

$$\mathbf{k}_{n_1, n_2}^{\pm} = (k_1 + n_1)\mathbf{d}_1^* + (k_2 + n_2)\mathbf{d}_2^* \pm k_{3, n_1, n_2} \mathbf{d}_3^*,$$

$$|\mathbf{k}_{n_1, n_2}^{\pm}| = \omega/c, \quad \arg(k_{3, n_1, n_2}) \in \{0, \pi/2\}. \quad (18)$$

The series (17) suppose that the media above and below the grating layer are homogeneous. Without loss of generality, we have assumed that this medium is the vacuum (18). We denote by  $E^{\sigma, \pm}$  the infinite column vector defining the tangential components  $E_{1, n_1, n_2}^{\sigma, \pm}$  and  $E_{2, n_1, n_2}^{\sigma, \pm}$  of the vectorial functions  $\mathbf{E}^{\sigma, \pm}$  for all  $\sigma = u, d$ :

$$E^{\sigma, \pm} = \begin{pmatrix} E_{1, n_1, n_2}^{\sigma, \pm} \\ E_{2, n_1, n_2}^{\sigma, \pm} \end{pmatrix}_{n_1, n_2 \in \mathbb{Z}}. \quad (19)$$

The  $S$  matrix links the vectors  $E^{u, +}$  and  $E^{d, -}$  [Eq. (19)] to the vectors  $E^{u, -}$  and  $E^{d, +}$  (Ref. 21):

$$\begin{pmatrix} E^{u, +} \\ E^{d, -} \end{pmatrix} = S(\omega, k_1, k_2) \begin{pmatrix} E^{u, -} \\ E^{d, +} \end{pmatrix} = \begin{bmatrix} S_{11} & S_{12} \\ S_{21} & S_{22} \end{bmatrix} \begin{pmatrix} E^{u, -} \\ E^{d, +} \end{pmatrix}. \quad (20)$$

Using the Rayleigh development [Eq. (17)], we define another transfer matrix  $\tilde{T}$ :

$$\begin{pmatrix} E^{u, +} \\ E^{u, -} \end{pmatrix} = \tilde{T}(\omega, k_1, k_2) \begin{pmatrix} E^{d, +} \\ E^{d, -} \end{pmatrix}. \quad (21)$$

Since the matrix  $\tilde{T}$  is linked with  $T$  by a change of basis, these matrices are isomorphic and have the same eigenvalues. From Eqs. (20) and (21), the expression for the matrix  $(\tilde{T}^{-1} \pm I)^{-1}$  is

$$(\tilde{T}^{-1} \pm I)^{-1} = \begin{bmatrix} S_{11}^{-1}(I_{11} \pm S_{12})\tilde{X} & -S_{11}^{-1}(I_{11} \pm S_{12})\tilde{X}S_{22}(I_{11} \pm S_{12})^{-1} \\ \tilde{X} & \tilde{X}(S_{21}S_{11}^{-1}S_{12} - S_{22} \pm S_{11}^{-1}S_{12}) \end{bmatrix}, \quad (22)$$

where  $I_{11}$  is the identity matrix and

$$\tilde{X} = (S_{21}S_{11}^{-1} \pm S_{11}^{-1} \pm S_{21}S_{11}^{-1}S_{12} \mp S_{22} + S_{11}^{-1}S_{12})^{-1}. \quad (23)$$

Note that we chose to use the matrix  $(\tilde{T}^{-1} \pm I)^{-1}$  instead of  $(\tilde{T} \pm I)^{-1}$  to obtain a simpler expression.

## 4. NUMERICAL RESULTS

In this section, we illustrate the algorithms (15) and (22) with the actual structures of face-centered-cubic woodpile and simple cubic photonic crystals. The structure parameters are chosen to fit the experimental realizations of the Sandia National Laboratories.<sup>23,25</sup> Both structures are constructed by using advanced silicon processing with a simple stacking scheme. They are promising, since they possess a full photonic bandgap and the technology allows the design of such structures at wavelengths in the near-infrared region.

Before giving the numerical results, we present the representation of the dispersion relation that we have adopted. This representation consists in projecting the unit cell of the dual lattice.<sup>9</sup>

Using the common symmetries of the two studied structures, we reduce the unit cell (5) of the dual lattice to the reduced unit cell (Fig. 4)

$$\begin{aligned} V_r^* &= \{\mathbf{k} = k_1\mathbf{d}_1^* + k_2\mathbf{d}_2^* + k_3\mathbf{d}_3^* \in \mathbb{R}^3 \\ & \quad k_1 \in [0, 1/2], k_2 \in [0, k_1], k_3 \in [-1/2, 1/2]\}. \end{aligned} \quad (24)$$

With our numerical approach, we fix the values of the frequency  $\omega$  and the two components  $k_1$  and  $k_2$  of the Bloch wave vector  $\mathbf{k}$ . The truncated matrix is  $N \times N$  and has  $N$  eigenvalues, which are computed by using the techniques described in Section 3. Two cases can occur. First, if there is no eigenvalue with modulus equal to 1, Eq. (12) cannot be fulfilled with a real Bloch wave vector  $\mathbf{k}$ . It means that there is no propagative solution, which is characteristic of a gap. Second, if there is at least one eigenvalue with modulus equal to 1, there is at least one propagative Bloch mode and its Bloch wave-vector component  $k_3$  is given by Eq. (12). The representation that we have adopted is the following: In the first case, we plot a gray point (gap), and in the other case, we plot a white point (propagative solution). Consequently, for each  $\omega$ , we vary the parameters  $k_1$  and  $k_2$  in the reduced unit cell projected onto the  $(k_1, k_2)$  plane (represented by the hatched triangle in Fig. 5). Finally, we restrict the scan of the projected reduced unit cell to its boundary  $\Gamma X M \Gamma$  (Fig. 5).

Even if this representation is simple, all the vertical faces of the reduced unit cell  $V_r^*$  (Fig. 4) are scanned. Consequently, the projection of the most degenerated points of the reduced unit cell  $V_r^*$  are contained in the boundary  $\Gamma X M \Gamma$ . Note that the diagrams obtained in

this way are different from the conventional ones, in which each mode is represented by a point on a line.

Now we are ready to present our numerical examples.

### A. Face-Centered-Cubic Woodpile Photonic Crystal

We consider here a structure realized experimentally by Lin *et al.*<sup>22,23</sup> and shown schematically in Fig. 6. This

woodpile photonic crystal is a stack of identical layers consisting of a periodic array of silicon rods with a rectangular cross section. Two consecutive layers are perpendicular, and two consecutive parallel layers are shifted by a half-period (Fig. 6). The resulting structure is face-centered tetragonal, and in the special case where  $d_{1,1} = d_{2,2} = \sqrt{2}d_{3,3} = a/\sqrt{2}$ , it is face-centered cubic. The relevant parameters of this structure are the index ratio [equal to 3.6 (silicon and air)]; the filling factor [equal to 0.28 (the ratio of the rod width to the horizontal spatial period)], and the length  $a$ .

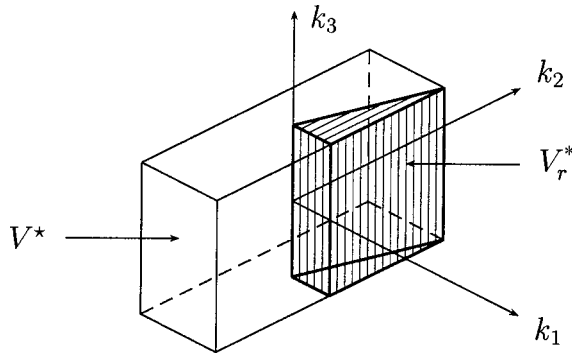


Fig. 4. Unit cell  $V^*$  of the dual lattice and the reduced unit cell  $V_r^*$  (hatched volume).

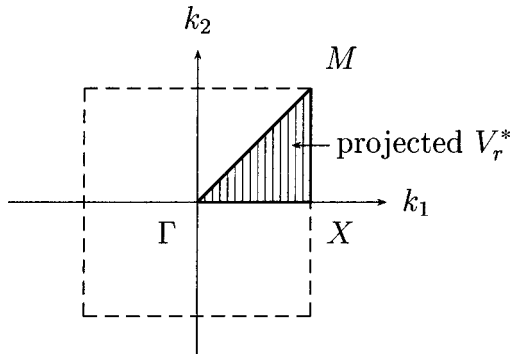


Fig. 5. Projected reduced unit cell of the dual lattice (hatched triangle) and its boundary  $\Gamma X M \Gamma$ .

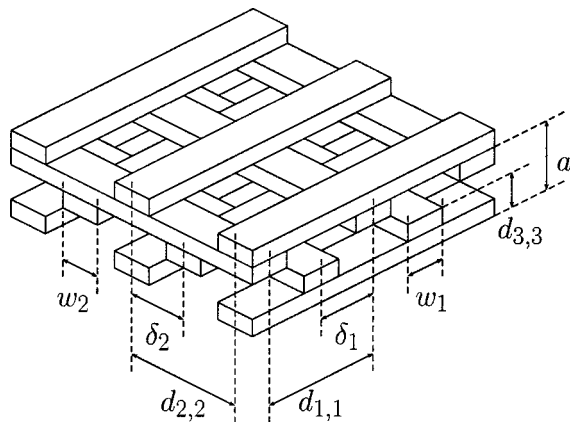


Fig. 6. Schematic representation of the face-centered-cubic woodpile photonic crystal. The horizontal spatial periods  $d_{1,1}$  and  $d_{2,2}$  are  $d_{1,1} = d_{2,2} = a/\sqrt{2}$ . The shifts  $\delta_1$  and  $\delta_2$  are equal to a half-period:  $\delta_1 = \delta_2 = a/(2\sqrt{2})$ . The silicon rods are of width  $w_1 = w_2 = 0.28d_{1,1} = 0.28d_{2,2}$  and of height  $d_{3,3}/2 = a/4$ .

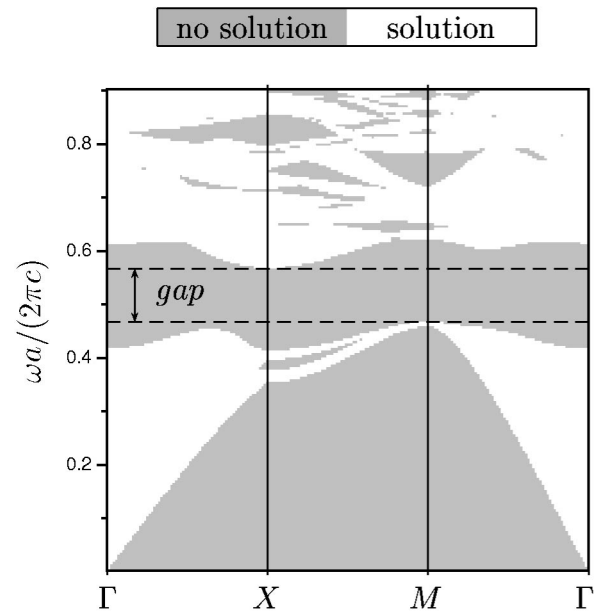


Fig. 7. Representation of the dispersion relation of the face-centered-cubic woodpile photonic crystal. Abscissa, projection of the Bloch vector  $\mathbf{k}$  onto  $\Gamma X M \Gamma$ ; ordinate, normalized frequency.

**Table 1. Upper and Lower Band Edges for Different Values of the Number of Functions Retained for the Computation**

Number of Functions	Upper Band Edge	Lower Band Edge	CPU Time <sup>a</sup> (s)
5 × 5	0.5675	0.4649	0.11
7 × 7	0.5680	0.4672	0.77
9 × 9	0.5689	0.4687	3.6
11 × 11	0.5698	0.4669	14
13 × 13	0.5700	0.4681	57
15 × 15	0.5696	0.4678	171
17 × 17	0.5698	0.4681	469
19 × 19	0.5700	0.4676	908

<sup>a</sup> CPU times in seconds for a one-point computation on a Compaq ds20e workstation (666-MHz Alpha processor).

Figure 7 shows the representation of the dispersion relation. We use in that case algorithm (15) based on the  $R$  matrix. We obtain the  $R$  matrix of the grating layer (which is made up of a stack of two orthogonal periodic arrays of rods) from the rigorous modal method used in grating theory<sup>17,18</sup> and generalized for conical mountings.<sup>19,20</sup> The main advantage of this method is that the permittivity  $\epsilon$  is strictly represented by a piecewise-constant function and not represented by a truncated Fourier series. A second advantage is that a small number of basis functions can represent the electromagnetic field with good accuracy. These two points make the convergence fast.

The dispersion relation in Fig. 7 shows that this crystal presents a full photonic bandgap for

$$\omega a / (2\pi c) \in [0.468 \pm 0.001, 0.569 \pm 0.001]. \quad (25)$$

This result confirms the previous theoretical estimations.<sup>10,23</sup> The given precision results from the

numerical study of the convergence of the values of the bandgap edges. Table 1 shows the behavior of the value of the band edges when the number of functions retained for the computation increases. Note that the total size of the eigenproblem is four times bigger than this number because of the four components of the tangential field. It is worth noting that algorithm (15) does not present any numerical instabilities. From Table 1, it is found that the number of  $5 \times 5$  functions gives results with a precision better than 0.5% when compared with the final values. With this small number of functions, the CPU time is only approximately 0.11 s for each fixed value of the three parameters  $k_1$ ,  $k_2$ , and  $\omega$ . For a complete dispersion relation as represented in Fig. 7 with  $150 \times 150$  points, the CPU time needed is approximately 42 min (close to the CPU time needed for 2D crystals).

### B. Simple Cubic Photonic Crystal

Now we study the simple cubic structure realized experimentally by Lin *et al.*<sup>25</sup> Figure 8 shows the unit cell of this crystal, composed of three identical square rods of silicon along the orthonormal spatial periods  $\mathbf{d}_1$ ,  $\mathbf{d}_2$ , and

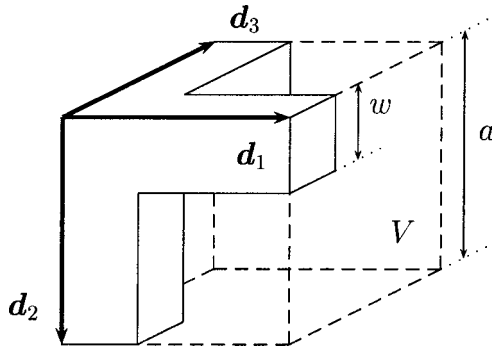


Fig. 8. Unit cell of the simple cubic photonic crystal.

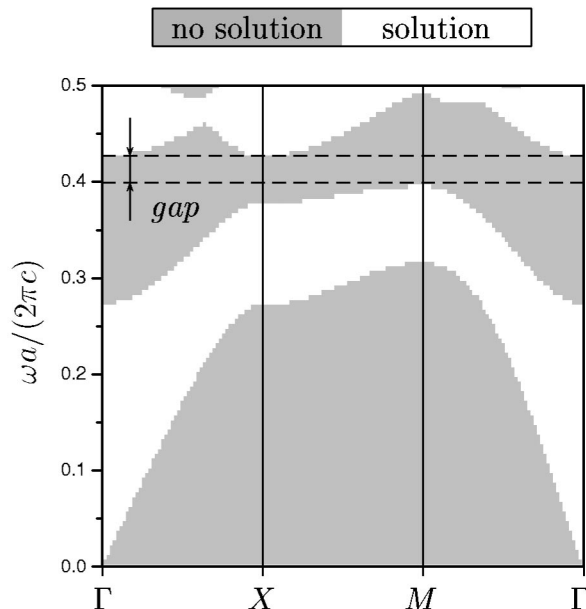


Fig. 9. Representation of the dispersion relation of the simple cubic photonic crystal. Abscissa, projection of the Bloch vector  $\mathbf{k}$  onto  $\Gamma X M \Gamma$ ; ordinate, normalized frequency.

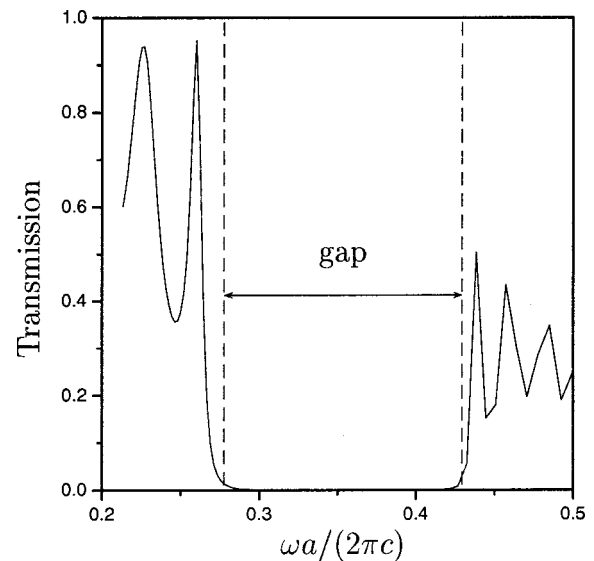


Fig. 10. Transmission through six identical grating layers for normal incidence ( $\Gamma$  point). The dashed lines [ $\omega a/(2\pi c) = 0.273$  and  $0.426$ ] are the limits of the gap corresponding to the infinite crystal in normal incidence, deduced from Fig. 9.

**Table 2. Upper Band Edge at the  $\Gamma$  Point (Normal Incidence) for Different Values of the Number of Functions Retained for the Computation**

Number of Functions	Upper Band Edge	CPU Time <sup>a</sup> (s)
$5 \times 5$	0.4362	0.32
$7 \times 7$	0.4281	2.3
$9 \times 9$	0.4266	9.6
$11 \times 11$	0.4268	33
$13 \times 13$	0.4265	95

<sup>a</sup> CPU times in seconds for a one-point computation on a Compaq ds20e workstation (666-MHz Alpha processor).

$\mathbf{d}_3$ . The index ratio is again 3.6, and the filling factor is equal to 19% (the width of the silicon rods is equal to 25% of the cube edge length:  $w = 0.25a$ ).

Figure 9 shows the representation of the dispersion relation. To illustrate the second algorithm [Eq. (22)], we use in this section the  $S$  matrix. Our code uses the Fourier modal method<sup>24</sup> to obtain the  $S$  matrix. This formulation takes care of the product of truncated Fourier series in order to improve the convergence.<sup>30</sup> The dispersion relation in Fig. 9 shows that this crystal presents a full photonic bandgap. Note that with our representation the “ $\Gamma X$ ” path corresponding to the normal incidence in Ref. 25 is concentrated on our  $\Gamma$  point. When compared with Fig. 1 of Ref. 25, the band edges of the full bandgap of Fig. 9 are shifted to higher frequencies. This discrepancy may explain the difference between transmission curve and dispersion relation in Ref. 25.

Figure 10 shows the transmission curve computed by using the same Fourier modal method and the limits of the gap for normal incidence ( $\Gamma$  point). Note that in the projected unit cell of Fig. 5, the normal incidence

( $k_1 = k_2 = 0$ ) corresponds to the  $\Gamma$  point only, whereas in the usual representation it corresponds to the  $\Gamma X$  line. The agreement with the transmission curve (Fig. 4 of Ref. 25) computed by using the transfer-matrix method is excellent, as is that with our dispersion relation represented in Fig. 9 (intersection of the gray region with the left vertical axis). Thus it appears that the discrepancy between theory and experiments in Ref. 25 is probably due to the slow convergence of the plane-wave method.

Finally, Table 2 shows that the second algorithm [Eq. (22)] is also stable and guarantees the precision of the computed value of the upper band edge of the gap at the  $\Gamma$  point (normal incidence).

## 5. CONCLUSION

We have presented two stable algorithms to compute dispersion relation diagrams from scattering or impedance matrices of a single grating layer. We think that the methods that we have presented in this paper are valuable tools in the domain of photonic crystal engineering. Practical applications of photonic crystals are now conceivable, and thus the need for accurate and reliable methods to study their optical properties exists. One of the advantages of the grating layer method is that it profits from the great amount of work done in the domain of diffractive optics and more precisely in the electromagnetic theory of gratings. In this domain, the usual applications require accurate numerical results for design of the structures, and thus numerical methods such as integral, differential, or modal methods are mature. With the presented algorithms, all these methods can be used for the computation of the dispersion relation of various kinds of photonic crystals, with use of the more adapted one depending on the geometry. We have shown the efficiency of our approach in the case of cubic-face-centered woodpile photonic crystals with a rigorous modal method and in the case of cubic simple photonic crystals with a Fourier modal method. The rigorous modal method adapted to woodpile structures gives us converged results (within 0.5%) with only  $5 \times 5$  basis functions and 0.11 s per computed point. With the Fourier modal method, we show again the relevance of the approach, with converged results with  $9 \times 9$  Fourier coefficients, while plane-wave methods fail to converge with the same structure and more than 1000 plane waves.

A decisive advantage of the approach is the possibility of using the same code to investigate various physical problems: dispersion relation, transmission, reflection and absorption by a finite stack of photonic crystal slices, emission of a dipole inside a limited photonic crystal, etc.

The corresponding author, Stefan Enoch, can be reached by phone, 33-491-288-376; fax, 33-491-674-428; or e-mail, stefan.enoch@fresnel.fr.

## REFERENCES

1. K. Ho, C. Chan, and C. Soukoulis, "Existence of photonic gap in periodic dielectric structures," *Phys. Rev. Lett.* **65**, 3152–3155 (1990).
2. J. Joannopoulos, R. Meade, and J. Winn, *Photonic Crystals* (Princeton U. Press, Princeton, N.J., 1995).
3. J. B. Pendry, "Photonic band structures," *J. Mod. Opt.* **41**, 209–229 (1994).
4. A. Moroz, "Density-of-states calculations and multiple-scattering theory for photons," *Phys. Rev. B* **51**, 2068–2081 (1995).
5. A. Moroz and C. Sommers, "Photonic band gaps of three-dimensional face-centered cubic lattices," *J. Phys. Condens. Matter* **11**, 997–1008 (1999).
6. R. C. McPhedran, L. C. Botten, A. A. Asatryan, N. A. Nicorovici, P. A. Robinson, and C. M. de Sterke, "Calculation of electromagnetic properties of regular and random arrays of metallic and dielectric cylinders," *Phys. Rev. E* **60**, 7614–7617 (1999).
7. B. Gralak, S. Enoch, and G. Tayeb, "Anomalous refractive properties of photonic crystals," *J. Opt. Soc. Am. A* **17**, 1012–1020 (2000).
8. L. C. Botten, N. A. Nicorovici, R. C. McPhedran, C. M. de Sterke, and A. A. Asatryan, "Photonic band structure calculations using scattering matrices," *Phys. Rev. E* **64**, 046603 (2001).
9. A. Modinos, N. Stefanou, and V. Yannopoulos, "Applications of the layer-KKR method to photonic crystals," *Opt. Express* **8**, 197–202 (2001).
10. D. M. Whittaker, "Inhibited emission in photonic woodpile lattices," *Opt. Lett.* **25**, 779–781 (2000).
11. R. Petit, "Contribution à l'étude de la diffraction d'une onde plane par un réseau métallique," *Rev. Opt. Theor. Instrum.* **6**, 263–281 (1963).
12. P. Vincent and M. Nevière, "Corrugated dielectric waveguides: a numerical study of the second-order stop bands," *Appl. Phys.* **20**, 345–351 (1979).
13. M. Nevière, R. Reinisch, and D. Maystre, "Surface enhanced second harmonic generation at a silver grating: a numerical study," *Phys. Rev. B* **32**, 3634–3641 (1985).
14. D. Maystre, in *Electromagnetic Theory of Gratings*, R. Petit, ed. (Springer-Verlag, Berlin, 1980), Chap. 3.
15. E. Popov and M. Nevière, "Grating theory: new equations in Fourier space leading to fast converging results for TM polarization," *J. Opt. Soc. Am. A* **17**, 1773–1784 (2000).
16. E. Popov and M. Nevière, "Maxwell equations in Fourier space: fast converging formulation for diffraction by arbitrary shaped, periodic, anisotropic media," *J. Opt. Soc. Am. A* **18**, 2886–2894 (2001).
17. L. C. Botten, M. S. Craig, R. C. McPhedran, J. L. Adams, and J. R. Andrewartha, "The dielectric lamellar diffraction grating," *Opt. Acta* **28**, 413–428 (1981).
18. L. C. Botten, M. S. Craig, R. C. McPhedran, J. L. Adams, and J. R. Andrewartha, "The finitely conducting lamellar diffraction grating," *Opt. Acta* **28**, 1087–1102 (1981).
19. S.-E. Sandström, G. Tayeb, and R. Petit, "Lossy multistep lamellar gratings in conical diffraction mountings: an exact eigenfunction solution," *J. Electromagn. Waves Appl.* **7**, 631–649 (1993).
20. L. Li, "A modal analysis of lamellar diffraction gratings in conical mountings," *J. Mod. Opt.* **40**, 553–573 (1993).
21. L. Li, "Formulation and comparison of two recursive matrix algorithms for modeling layered diffraction gratings," *J. Opt. Soc. Am. A* **13**, 1024–1035 (1996).
22. S. Y. Lin, J. G. Fleming, D. L. Hetherington, B. K. Smith, R. Biswas, K. M. Ho, M. M. Sigalas, W. Zubrzycki, S. R. Kurtz, and J. Bur, "A three-dimensional photonic crystal operating at infrared wavelengths," *Nature (London)* **394**, 351–353 (1998).
23. J. G. Fleming and S.-Y. Lin, "Three-dimensional photonic crystal with a stop band from 1.35 to 1.95  $\mu\text{m}$ ," *Opt. Lett.* **24**, 49–51 (1999).
24. L. Li, "New formulation of the Fourier modal method for crossed surface-relief gratings," *J. Opt. Soc. Am. A* **14**, 2758–2767 (1997).
25. S.-Y. Lin, J. G. Fleming, R. Lin, M. M. Sigalas, R. Biswas, and K. M. Ho, "Complete three-dimensional photonic band-gap in a simple cubic structure," *J. Opt. Soc. Am. B* **18**, 32–35 (2001).

26. H. Sözüer, J. Haus, and R. Inguva, "Photonic bands: convergence problems with the plane-wave method," *Phys. Rev. B* **45**, 13962–13972 (1992).
27. F. Montiel and M. Nevière, "Differential theory of gratings: extension to deep gratings of arbitrary profile and permittivity through the *R*-matrix propagation algorithm," *J. Opt. Soc. Am. A* **11**, 3241–3250 (1994).
28. D. Maystre, "Electromagnetic study of photonic band gaps," *Pure Appl. Opt.* **3**, 975–993 (1994).
29. R. Petit, ed., *Electromagnetic Theory of Gratings* (Springer-Verlag, Berlin, 1980).
30. L. Li, "Use of Fourier series in the analysis of discontinuous periodic structures," *J. Opt. Soc. Am. A* **13**, 1870–1876 (1996).